Fourth International Symposium on Marine Propulsors
smp'15, Austin, Texas, USA, June 2015

Investigation of the propeller slip stream over an Azipod propulsor by PIV measurements and CFD simulations

Andrei Korsström[1], Pasi Miettinen[1], Satu K. Hänninen[2], Keijo Hanhirova[3]

[1] ABB Marine and Ports, P.O. Box 185, FI-00981 Finland
[2] Department of Applied Mechanics, School of Engineering,
Aalto University, P.O. Box 12200, FI-00076 Aalto, Finland.
Presently: VTT Technical Research Centre of Finland,
P.O. Box 1000, FI-02044 VTT, Finland
[3] Department of Civil and Structural Engineering, School of Engineering,
Aalto University, P.O. Box 12100, FI-00076 Aalto, Finland

1 ABSTRACT

In the following study the possibility to simulate the propeller slip flow over a pod propulsor has been investigated. The slipstream can be investigated either through measurements or by calculations. Since the measurements had to be done in model scale all the comparisons have been done in that scale.

For this study a pod unit with a working propeller was experimentally investigated using the particle image velocimetry (PIV) method. This was done at two different advance ratios. The same condition was then investigated both with a boundary element method (BEM) and Unsteady Reynolds Averaged Navier-Stokes (URANS) calculations. In the URANS approach both SST (Menter) k-ω and Reynolds stress transport (RST) turbulence models were used. The RST model takes into account the anisotropy of turbulence.

From the calculation methods there are clear differences in the approach. The BEM has its unknowns on the surface only and computes field quantities as a post-processing step. The URANS on the other hand incorporates calculation cells between the calculation surfaces and the plane of interest, and hence, takes into account the volume of the fluid.

Keywords

Pod propulsor, Particle Image Velocimetry PIV, Boundary Element Method BEM, Unsteady Reynolds-Averaged Navier-Stokes URANS

2 INTRODUCTION

In internal studies at ABB, it has been concluded that we can achieve a suitable accuracy in regards to propeller thrust and torque around the design point, with the BEM and URANS calculations. However, to catch the rotational energy lost by the motion of the propeller an interest has grown in how well the slip stream from the propeller can be simulated over the Azipod housing. The capability of the numerical methods to do this is studied by comparing the numerical results with the experimental results given by PIV measurements.

PIV measurements have earlier been used, for instance, when investigating the flow field from the propeller over a rudder (for instance Felli *et al.* 2011) but not to our knowledge for a pod. Additionally, the slip stream of a propeller has been compared to URANS calculations by Roosenboom *et al. (2009)*

3 CONDITIONS

The investigations were made over the Azipod unit at two different advance ratios (0.8 and 0.9) defined by Equation (1). Here the rotation rate (n) was 15 Hz and the propeller diameter D approximately 230 mm. Equation (1) was used then to define the inflow speed to match the advance ratio.

$$J = {}^{V}/_{nD} \qquad (1)$$

For the setup the Reynolds number

$$R_n = \sqrt{V^2 + (0.7R2\pi n)^2} \cdot {}^{c}/_{\nu} \qquad (2)$$

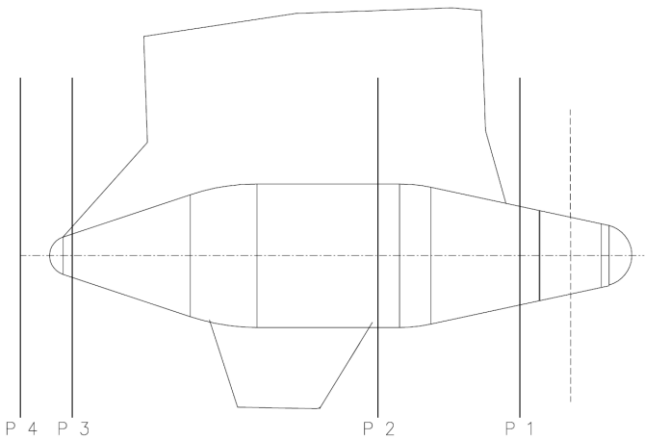

Figure 1 Measurement planes along the Azipod body

was 5.4 and 5.5 $\cdot 10^5$ over the 0.7 radius chord (c) as the kinematic viscosity was $\nu = 1.14 \cdot 10^{-6}$ m^2/s.

The unit was located in a uniform inflow which corresponds to an open water condition. The slip flow was investigated at four locations along the propeller axis of the unit (Figure 1).

3.1 Analysis

All the methods, have different grids in the planes where the results are compared. To compensate for this the results were first interpolated to the same nodes defined in Figure 2. The axial velocity component (along the propeller axis) was compared at the nodes of the green mesh with a contour plot. The velocity vectors for the cross flow, i.e. vectors shown in the current plane, were drawn at the dots shown in Figure 2, where the two larger black circles represent the propeller and

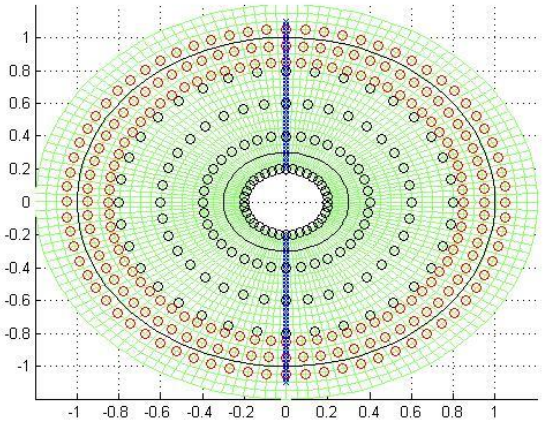

Figure 2 Grid used in comparisons

the hub. Additionally, the direction of the inflow for the fins was calculated from the horizontal cross component and the axial component at the blue lines given at 6 and 12 o'clock using Equation (3)

$$\alpha = tan(^{v}/_{u}), \qquad (3)$$

where v and u are the vertical and the horizontal components, respectively, Further the calculated flow fields are compared to the measured field. As the data is interpolated to the same grid, the differences in the non-dimensional velocity components can be compared with Equation (4), where i refers to the coordinate direction in question.

$$\Delta V_i = \left(^{V_{Calculated,i}}/_{V_{Measured,i}}\right) - 1 \qquad (4)$$

4 METHODS

4.1 Boundary Element Method

The boundary element method was developed within the Cooperate Research Ships (CRS) and the main focus has been on propeller calculations. However, with the software in question (Procal) a functionality to calculate propulsion units consisting of both rotating and stationary parts has been incorporated. In regards of the pod it means that it is an iterative calculation between a rotating and a stationary object coupled through the induction velocities from one object on the other. The rotational- and the stationary calculation are both independent routines, taking the induction velocity from the other object into account in the inflow velocities. So the result from the rotational routine is the trailing wake from the propeller, which does not take into account any components behind the propeller and therefore moves right through them.

For the present computations a prescribed geometry of the trailing wake has been used in which the pitch and contraction are prescribed using empirical formulations depending on pitch, advance ratio and skew. The influence of the stationary body is taken into account by modifying the ship wake field.

On the other hand the stationary calculation takes into account the induced velocity components computed at its collocation points of the stationary object. However, the stationary calculation does not show the result from the rotational calculation in its output. In order to investigate a flow field at a specified location, the field has to be calculated by both the rotational and the stationary routine and combined by assuming it to be the sum of the induction velocities of the two objects.

4.2 Unsteady RANS approach

Unsteady Reynolds-Averaged Navier-Stokes (URANS) sliding mesh approach is applied here. Commercial CFD code StarCCM+ version 9.02.005 is used. In URANS approach, an additional term, Reynolds stress tensor $\boldsymbol{T_t}$, is added in the momentum transport equation (StarCCM+ 9.02 User Guide)

$$\mathbf{T}_t \equiv -\rho\overline{\mathbf{v}'\mathbf{v}'} = -\rho\begin{bmatrix}\overline{u'u'} & \overline{u'v'} & \overline{u'w} \\ \overline{u'v'} & \overline{v'v'} & \overline{v'w'} \\ \overline{u'w'} & \overline{v'w'} & \overline{w'w}\end{bmatrix} \qquad (5)$$

Eddy viscosity model uses turbulent viscosity μ_t to model the Reynolds stress tensor:

$$\mathbf{T}_t = 2\mu_t\,\mathbf{S} - \frac{2}{3}(\mu_t\nabla\cdot\mathbf{v} + \rho k)\mathbf{I} \qquad (6)$$

where **S** is the strain tensor:

$$\mathbf{S} = \frac{1}{2}(\nabla\mathbf{v} + \nabla\mathbf{v}^T) \qquad (7)$$

and k is the turbulent kinetic energy. SST (Menter) k-ω turbulence model is used for solving additional transport equations for turbulent kinetic energy and specific dissipation rate ω that enable turbulent viscosity to be derived.

By solving all the components of the Reynolds stress tensor $\boldsymbol{T_t}$, Reynolds stress transport (RST) model is used for accounting effects of turbulence anisotropy, streamline curvature and rapid changes in the strain rate. The RST models are the most complex turbulent models in StarCCM+ since seven additional equations must be solved (compared to two equations in the SST (Menter) k-ω model). Six equations are needed for Reynolds stress tensor and one model equation for the isotropic turbulent dissipation ε.

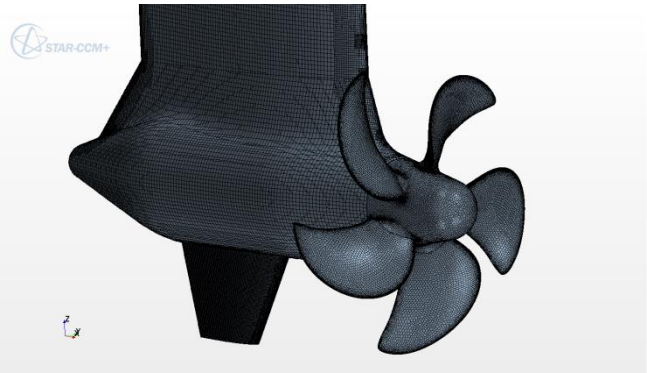

Figure 3 Mesh resolution on pod and propeller surfaces.

Rotating propeller region is meshed with polyhedral cells and prism layers and stationary pod region with trimmer cells and prism layers. Figure 3 shows mesh resolution on pod and propeller surfaces. Total number of cells in the simulation domain is approximately 6 million.

4.3 Experimental approach

4.3.1 Instrumentation

The experiments were performed in the towing tank of the Department of Applied Mechanics of Aalto University. The velocity field around the model of the Azipod unit was measured using a LaVision stereo-PIV system.

The velocity field was measured at four measurement planes (Figure 1). At each plane, the measurement was repeated at six blade positions for two advance ratios. In order to get a sufficient number of pictures (about 280), each test run with the towing carriage was repeated two or three times. Due to the applied measurement setup, only port side of the planes one and two could be measured, because the pod blocked out the view of the starboard side of the plane. Therefore, the flow field around the symmetric pod was captured by repeating the measurements both with the right- and left-handed versions of the propeller. Furthermore, the velocity field without the pod was measured in order to get information on the false velocities e.g. due to optical effects.

Figure 4 gives an overall view of the measurement setup. The Azipod unit was supported by the towing carriage below an underwater horizontal plate (A) that prevented wave generation in the vicinity of the Azipod. The underwater housing (B in Figure 4 and detailed in Figure 5) with the cameras and the sheet optics was located on the port side of the Azipod. The tubes, which support the housing, were equipped with freely rotating streamlined profiles (C) in order to prevent generation of von Karman vortex shedding that could cause vibrations of the housing. The model of the Azipod was equipped with turbulence stimulator strips behind the propeller and behind the leading edge of the strut.

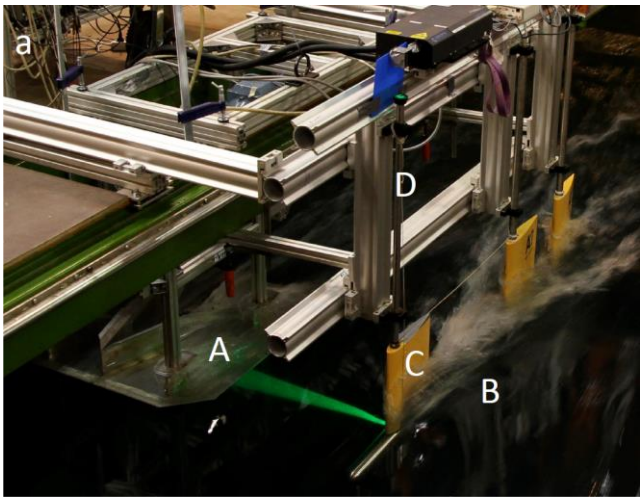

Figure 4 Measurement setup.

The laser (*New Wave Research* double pulse) was located above the underwater housing. The laser beam was first directed into the sheet optics down the forward tube (D in Figure 4) and then to the measurement area through an opening on the side of the forward section of the housing (E

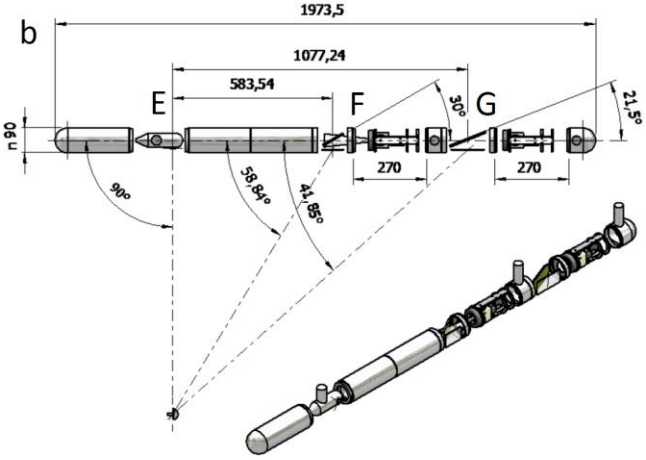

Figure 5 Underwater housing

in Figure 5). Two cameras (double frame *Imagerpro 4M*) and lenses (Canon 50 mm f1.4) equipped with Scheimpflug plane of focus adjustment mechanics were located in the aft section of the housing (F and G in Figure 5). The measurement was synchronized with the rotation angle of the propeller using a triggering device attached to the axis of the electrical motor running the propeller. The seeding system was located about 20 propeller diameters in front of the Azipod and fed the

mixture of hollow glass spheres with a diameter of 8-10 µm and water (volumetric ratio of roughly 100) to the flow.

The system was calibrated using a standard 20 by 20 cm calibration plate of *Type* 20 from *LaVision*. The measurements were performed with *DaVis* 7.2 imaging software.

4.3.2 Analysis of the experimental data

The first part of the analysis was performed with *DaVis* 7.2 imaging software. Each image was processed with the stereo-PIV cross-correlation routine. A multi-pass routine was applied so that the cross-correlation routine started with a larger interrogation window (size 64 times 64 pixels with 75 percent overlap) to get an initial guess for the velocity field and used a smaller window (32 times 32 pixels with 50 percent overlap) to resolve the final velocity field. The double pass was performed for both window sizes. This analysis was repeated for all individual measurements at each blade position and resulted in sets of instantaneous three dimensional velocity fields. The result at one blade position is the average velocity field of these sets. The average of the velocity fields at different blade positions gives the time averaged velocity field for the measurement plane in question.

The second part of the analysis was performed with Matlab. First, each velocity component was corrected by subtracting the corresponding component of the velocity field (correction field) that was measured without the pod. Before the correction, the advance velocity had been subtracted from axial velocity component of the correction field. In addition, the distribution of each component of the correction field was smoothened and the correction field was interpolated using a spline interpolation to the same points where the flow field around the pod was measured. Finally, the results of the left-handed propeller were mirrored to the starboard side of the measurement plane and combined to the results of the right-handed propeller to produce a complete flow field.

4.3.3 On the uncertainty of the experimental results

The measurement setup includes several sources of uncertainty that relate both to mechanical and optical details. One source of the uncertainty is a probable difference in pitch settings between the left- and right-handed propellers. The effects of some sources were minimized by the analysis. The choice of a high (75% instead of 50%) overlap of the interrogation window in the first pass of the analysis reduces the uncertainty caused by vibration of the Azipod unit during the measurements. The subtraction of the correction field reduces the uncertainty caused by the optical sources.

5 RESULTS

The results are studied one plane at a time. Since the first plane (P1 in Figure 1) behind the propeller, has the most rotational energy left and is closest to the influence of the change in the flow field, most of the comparisons between the results of the applied methods are presented in that plane.

The URANS results are generally calculated with the k-ω turbulence model, except in 5.1.2 where the impact of the turbulence model is investigated. Since the aim of the study was to compare the accuracy of the calculated results to the measured value, the difference is shown, where it yielded the clearest picture of the case (P1 and P2).

5.1 Plane one (P1)

The strut of the pod has an influence on the velocity field so the PIV measurements were concentrated on the upper part of the propeller disc. This is also clearly seen in the comparisons as the lower part of the propeller disc is missing.

5.1.1 Average flow field

In the figures, the contour plot represents the difference in the axial component and the scale is limited to ± 50 % of the measured result, due to this limitation the extreme values are not shown as colors, but indicated by the contours in the homogeneous color field. The vectors represent the change on the plane in question. The scale of the vectors is shown by the red line in the upper right corner which represent 10 % difference.

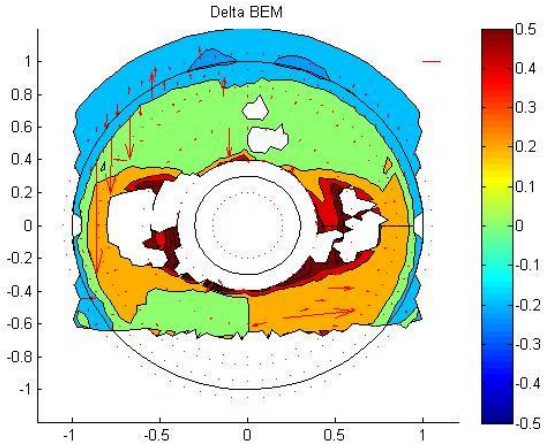

Figure 6 Difference in average velocity fields between BEM and PIV at P1

Figure 6 shows the difference between the velocities calculated with the BEM compared to the velocity measured with the PIV method.

Figure 7 shows the same difference, but in this case between the URANS result and the PIV measurement.

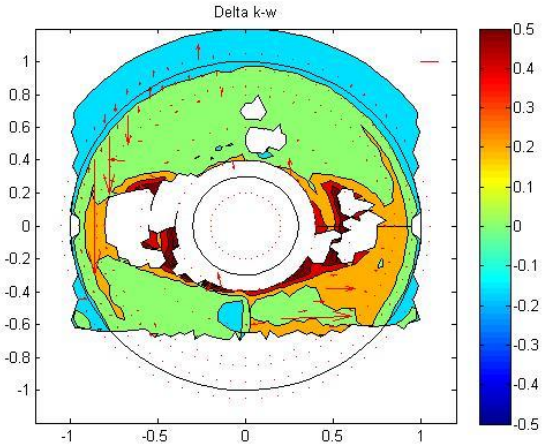

Figure 7 Difference in average velocity fields between URANS and PIV at P1

Based on Figure 6 and 7, the trend in the velocities is quite well predicted both with BEM and URANS (general trend within 15 %). Figure 8 shows an influence of the strut, which is also caught by the calculations as there is an even color distribution at the 12 o'clock position in Figures 6 and 7. In the lower part of the measurement plane there is a velocity step (Figure 8), not due to the fin, but due to a differences in results between the right and left handed propellers. This measurement discrepancy can also be seen in Figure 9, where the inflow to the strut is shown. The dotted line represent the results from the left handed and the dashed from the right handed propeller. The solid line for the PIV results is the average of the two.

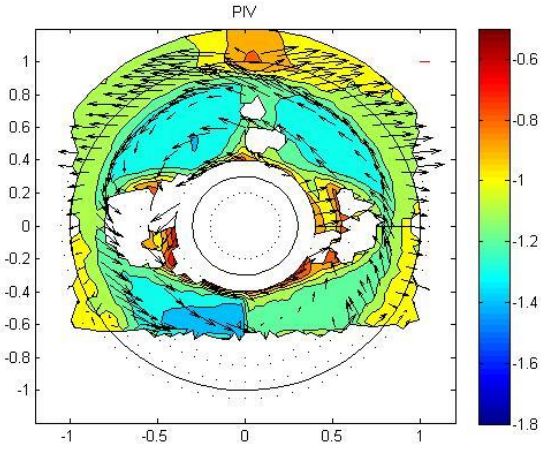

Figure 8 Non-dimensional velocity measured with PIV at P1

Figure 8 shows the non-dimensional velocity measured with the PIV method at plane one. The velocities are divided by the inflow velocity to express them in a non-dimensional form, the red line in the upper right corner represents 10 % of the inflow velocity and shows the scale of the vectors. The measurement results show quite strong vortices at the sides

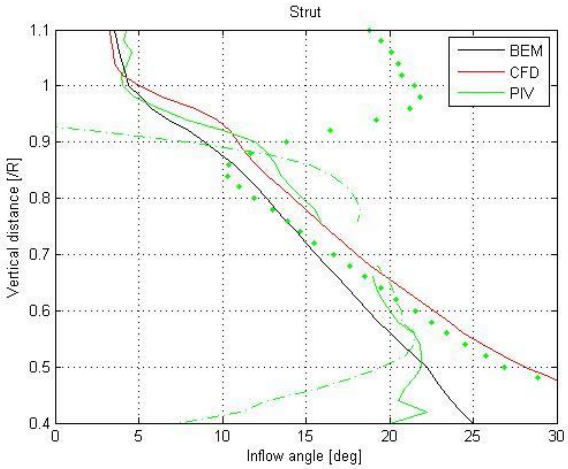

Figure 9 Inflow angle at 12 o'clock position at P1

of the motor tube and also a strong presence of the tip-vortex. When taken into account the strength of the tip-vortex in Figure 8, the lack of difference in the vectors in the tip region in both Figure 6 and 7 indicates that this region is also caught by the calculations.

Figure 9 shows the inflow angle at the 12 o'clock position, which would correspond to the strut leading edge, the URANS is really close to the average PIV measurement. The BEM calculation has a slight under prediction compared to the measurements.

5.1.2 Instantaneous flow field

To investigate the instantaneous flow field three URANS calculations were done, one with the k-ω model and two with the Reynolds Stress Transport model, both linear and

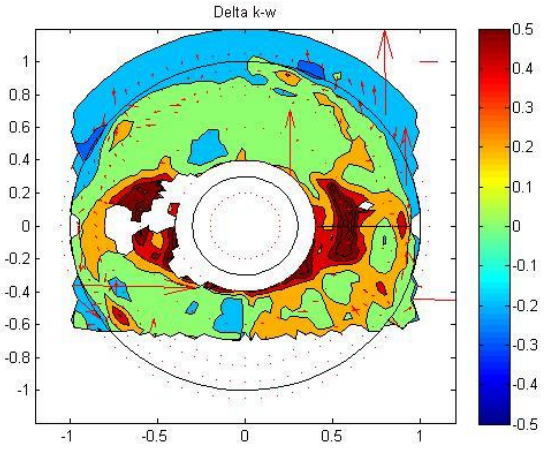

Figure 10 Difference in the instantaneous velocity fields between k-ω turbulence model and PIV at P1.

quadratic. (In the averaged flow field there was no significant difference depending on the turbulence model).

Figure 10, 11 and 12 show that both turbulence models give instantaneous results, which are close to each other. The results in the upper part of the propeller disc are slightly closer to the measured results in RST models, both for the axial velocity and vectors on the plane (1 – 2 o'clock). None of the URANS calculations catch the swirls at the sides of the motor tube, hence the figure show a pronounced difference between the computed and measured results in the area at 3

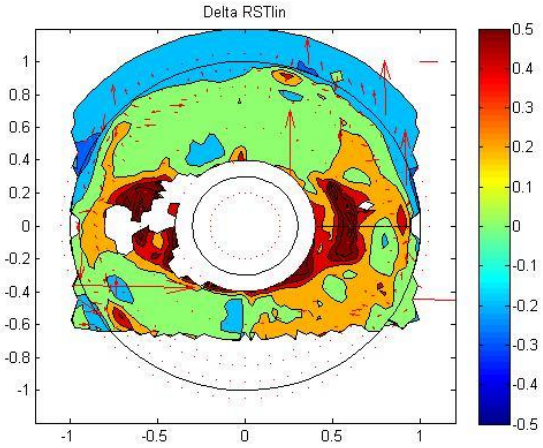

Figure 11 Difference in the instantaneous velocity fields between linear RST turbulence model and PIV at P1.

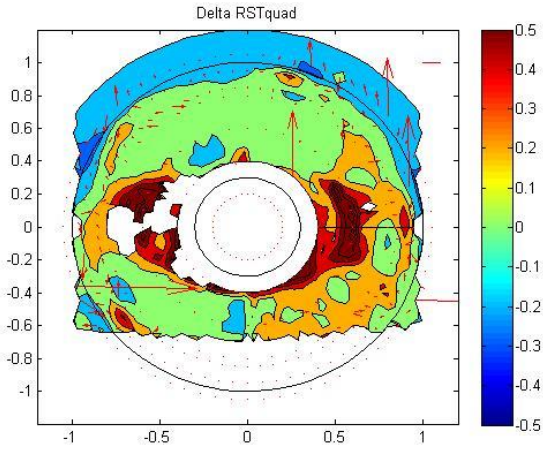

Figure 12 Difference in the instantaneous velocity fields between quadratic RST turbulence model and PIV at P1.

and 9 o'clock positions. The differences between the turbulence models are so small that this does not justify using the more time consuming RST models.

Figure 13 shows that the BEM results have a larger difference compared to the experimental results than the URANS results. As seen in the average flow field (Figure 13) the axial component given by BEM is slightly larger than measured by PIV. There are also larger differences in the tip region as the BEM does not calculate the tip-vortex, only the velocities at the blade surface.

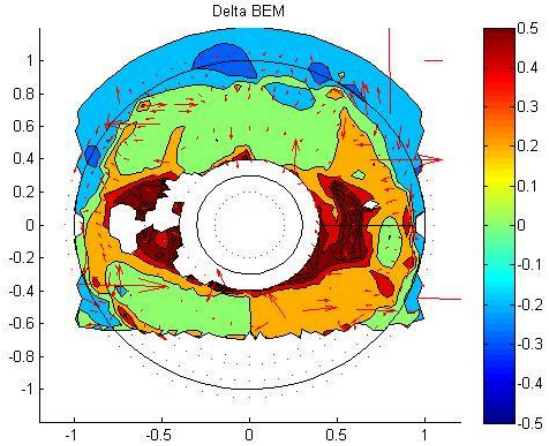

Figure 13 Difference in velocity fields between BEM and PIV at P1

5.1.3 Higher advance ratio

To compare the behavior at a slightly less loaded condition, the same tests and calculations were performed at a higher advance ratio of 0.9.

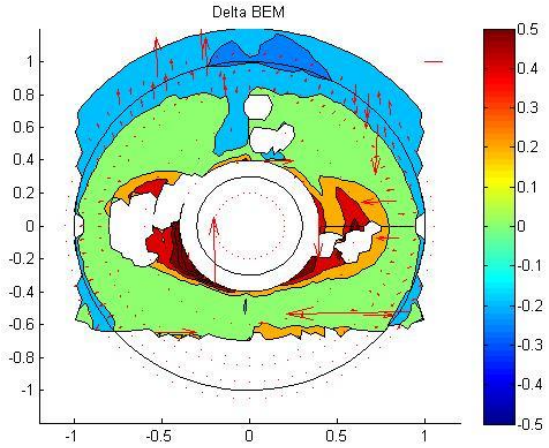

Figure 14 Difference in average velocity field between BEM and PIV at J = 0.9 at P1

Comparing the BEM results for the two advance rations, the differences in relation to the PIV results (Figure 6 and 14), and the influence of the strut is better caught with the lower advance number. But the area at the sides of the motor tube is, to the contrary, better caught with the higher advance number.

Due to the smaller swirl in the measurements, the URANS results are also comparably better (Figure 15). Similarly the velocity vectors at the tip also seem to be better predicted, especially in the 9 o'clock position.

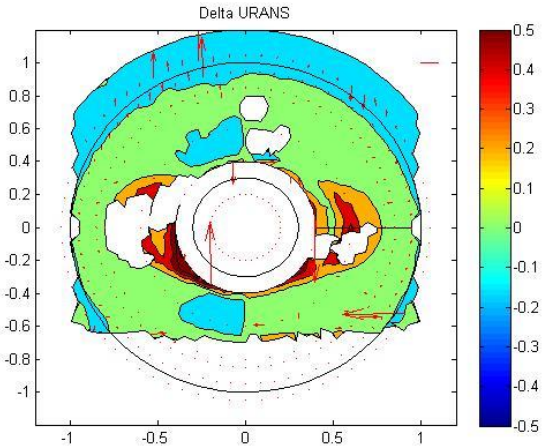

Figure 15 Difference in average velocity field between URANS and PIV at P1 at J = 0.9

Regarding the inflow angle (Figure 16), the measurements are influenced by the boundary layer around the motor, otherwise the values are about the same as for the lower advance ratio. For both calculation methods the inflow angle

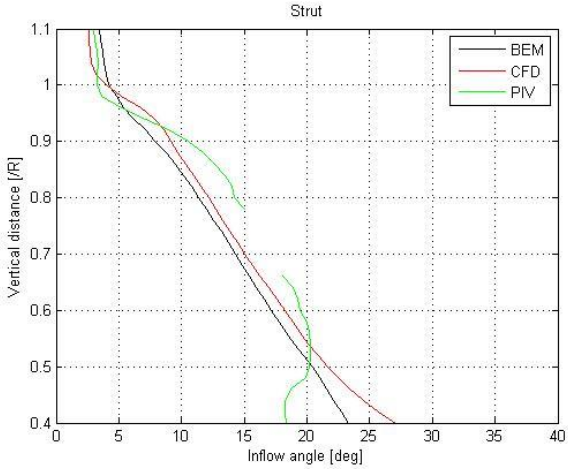

Figure 16 Inflow angle at 12 o'clock position at P1 and J = 0.9

decreases over the whole range. And it is even more pronounced for the URANS calculations than for the BEM results (Figure 16).

5.2 Plane two (P2)

The second plane represents the inflow to the fin below the motor tube. In this case the focus will be on the advance ratio 0.8, average flow field and the k-ω turbulence model in the URANS calculations. Here the PIV measurements were concentrated on the lower part of the propeller disc, which can also be seen in the comparison of the results. The side swirls that could be seen in plane one (Figure 8) are also present here.

Similar to Figure 6, Figure 17 shows that the axial velocity given by BEM is larger than that given by the experiments at

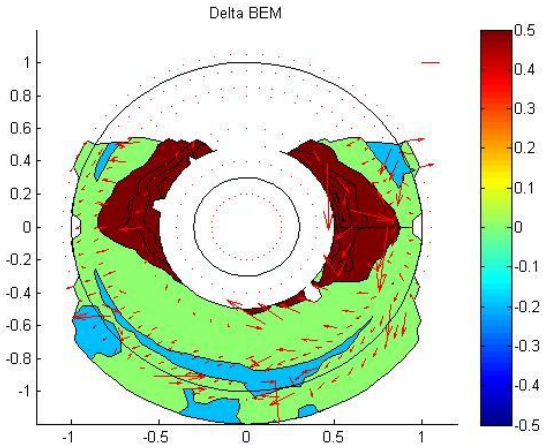

Figure 17 Difference in average velocity field between BEM and PIV at P2 at J = 0.8

the sides of the motor tube. Similarly the vectors start to grow which indicates that the difference in the planar velocity between the predictions given by BEM and the experiment is larger than the difference in plane one.

The change in the slipstream flow between the propeller and the stationary body is prescribed by empirical formulations, hence assuming that the flow will behave in a predefined way. For this reason it can be expected that the calculation accuracy will decrease when moving further away from the source of the induced velocity.

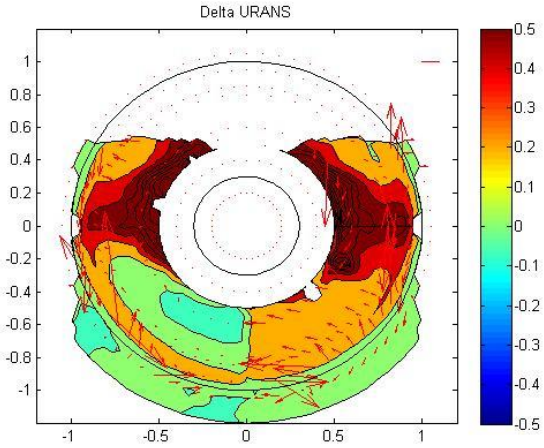

Figure 18 Difference in average velocity field between URANS and PIV at P2 at J = 0.8

The over prediction of the axial velocities for the URANS is larger for plane two than it was for plane one (Figure 7 and 18). The main reason are the swirls at the sides of the motor tube which were not predicted by the calculations.

The inflow angle to the fin (Figure 19), gives a similar slope for the two calculation methods. The measured values seem to have a strong side velocity around the tip of the fin, for which a slight indication is seen in the URANS calculation. Similarly to plane one the results measured with the left and right handed propellers are also shown. Noticeable is that the

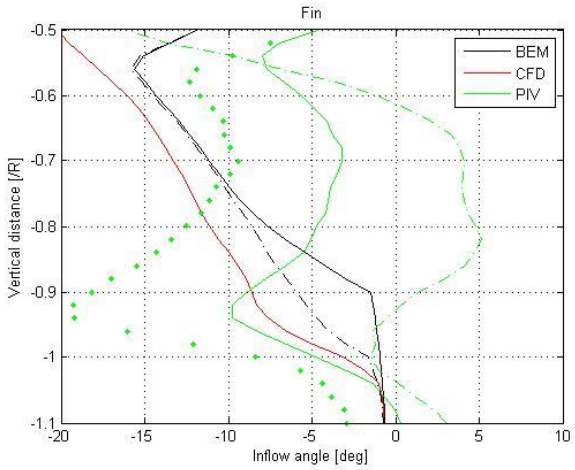

Figure 19 Inflow angle at 6 o'clock at P2

right handed propeller actually gives positive inflow angle, whereas both the left handed and the calculations predict a negative inflow angle. The BEM is influenced by the contraction factor for the prescribed wake geometry. The inflow predicted by BEM without the contraction is shown with the dashed line, which is a better prediction for the inflow angle, but gives a worse result for the propeller disc in the tip region.

5.3 Plane three (P3)

The third plane is just at the aft tip of the motor tube, so the influence of both the strut and the fin should be seen in the flow field. The measured velocity field (Figure 20) shows a strong influence of the strut, where the right hand side

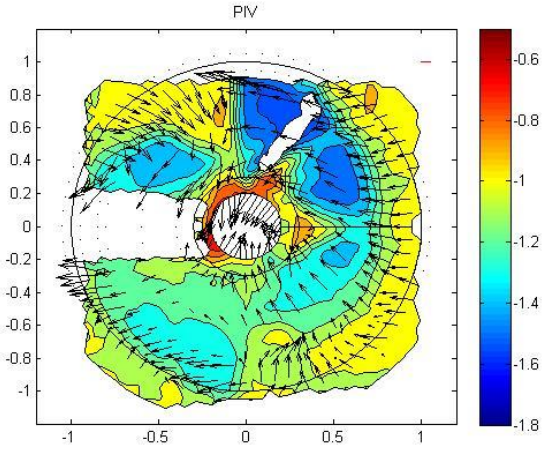

Figure 20 Velocity components measured at P3 with PIV

velocity is 1.5 compared to 1.0 on the left hand for the 12 o'clock position. The vector field has a lot more fluctuation than at the previous measurement planes, this is due to the shape change of the Azipod housing. Additionally, the total velocity vector would seem to be directed horizontally from right to left. This can also be seen in Figure 23, where the inflow angles are compared. The whole velocity field is measured with the right hand propeller, so there is no gap due to different propellers present.

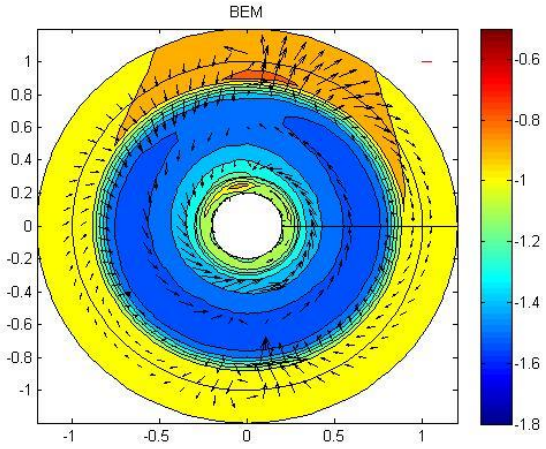

Figure 21 Calculated velocities at P3 with BEM

The velocity field calculated with the BEM (Figure 21), shows a radially homogenous field, so no peaks at 12 or 6 o'clock positions. However, the velocity vectors in the propeller tip region show an influence from the structures, and the magnitude of the velocity vectors are clearly increasing in the tip region, compared to the lower radii of the propeller disc.

The URANS (Figure 22) computations give a high influence of the strut and fin. The axial velocity field is of the same magnitude as the maximum measured, but the maximum is

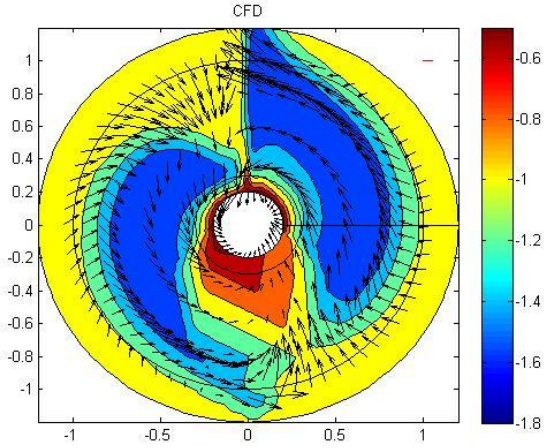

Figure 22 Calculated velocities at P3 with URANS

clearly distributed over larger area compared to the measured result. The velocity vectors are not as turbulent as on the measured plane, but have the same trend, i.e. apart from the rotational component, a clear inflow towards the disc center at the 5 and 11 o'clock positions.

For a rotational flow the expected inflow angle at the 12 and 6 o'clock position would be similar in size but of different sign, so for instance positive at 12 and negative at 6 o'clock. This has also been the case for planes one and two. The same can be seen for the URANS calculation (Figure 23) in plane three. Contrary to the assumption on how the flow would be aligned, the measured inflow angle is actually positive for both the 12 and 6 o'clock position. For the BEM calculations the plane is clearly too far and there is too much fluctuation in the result which seem to be due to the induced velocity from the stationary object i.e. the pod housing. The dotted black line is the inflow angle due to the rotational component without the contraction factor.

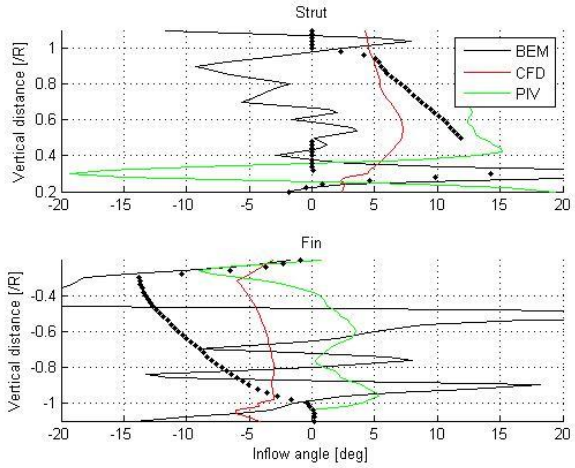

Figure 23 Inflow angle at P3 for 12 and 6 o'clock position.

5.4 Plane four (P4)

The last plane is located just behind the aft tip of the pod body. On this plane the swirl produced by the propeller around the pod housing should be present with some influence of the strut and fin.

The measured results (Figure 24) are similar to the results for plane three, but the largest velocity components have rotated over to the lower left quarter. The velocity vectors are starting to concentrate to a swirl around the center of the propeller disc. The rotation has also changed the direction of the total velocity vector, so that it would now seem to be more in a left to right direction. This can also be seen in Figure 27. For the measurements the left handed propeller was used. Taken the difference seen between the results of the left and right handed propeller (Figure 9 and 19) a change compared to the results on plane three (Figure 23) could be expected.

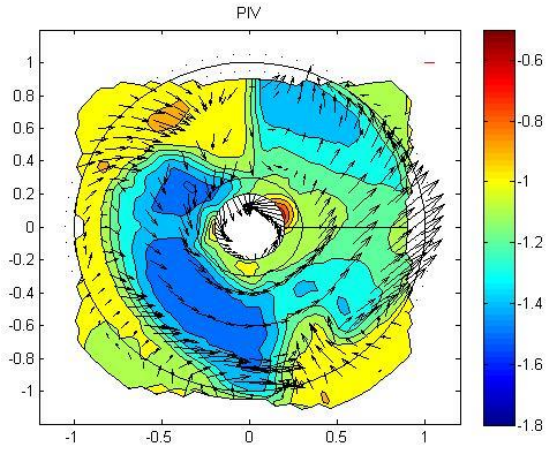

Figure 24 Velocity components measured at P4 with PIV

The BEM results (Figure 25) are similar to the results at plane three, a slight increase in the toroid slice at the center of the propeller disc and a decrease in axial velocity outside the propeller disc. This is due to the contraction function which is included in the calculation method for the trailing wake.

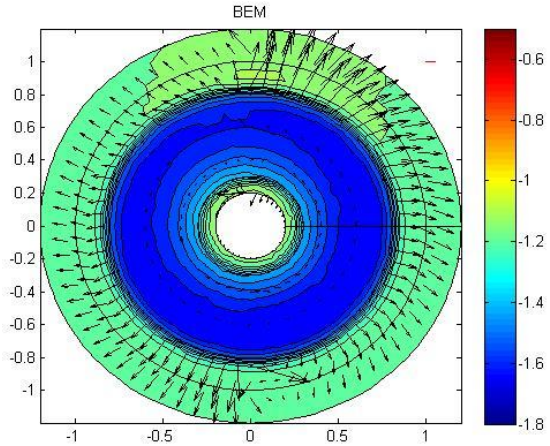

Figure 25 Velocity components measured at P4 with BEM

The lower left quadrant of the URANS results (Figure 26) has closed in the gap at the 6 o'clock position, and the axial flow has lost some of its intensity. The planar velocity vectors are still strong and pressing wedges into the fast slip stream form.

The inflow angle of the URANS calculation is similar to the one on plane three, but slightly shifted to the left (Figure 27). The BEM calculations show again a lot of fluctuation, but the results for the rotational component is similar to the result for

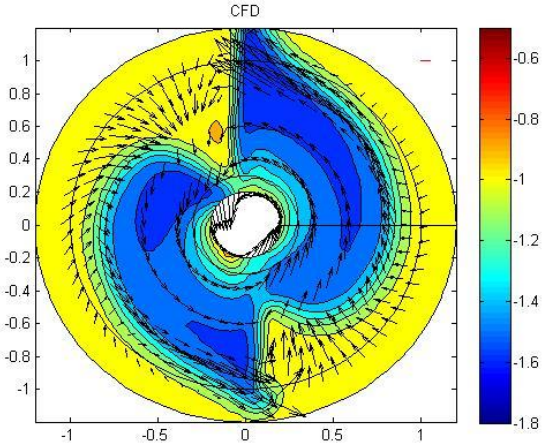

Figure 26 Velocity components measured at P4 with URANS

plane three. For the measurements there are some fluctuation, but generally a stable result. The inflow angle has shifted form plane three by approximately 15 degrees, which is in line with the difference seen in plane one and two for the two propellers. The shift has however, change the inflow angle from a positive to a negative, but the trend of both the 6 and 12 o'clock position having the same sign holds.

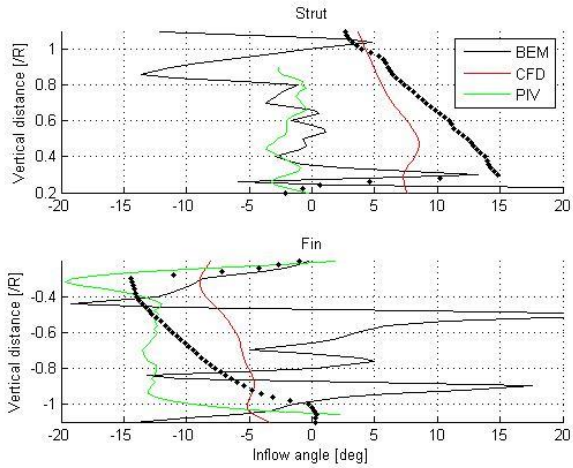

Figure 27 Inflow angle at P3 for 12 and 6 o'clock position.

6 Conclusions and discussion

The flow field over an Azipod unit was measured and compared to calculated results. The main investigation was done at advance ratio of 0.8, additionally the same comparison was done at a higher advance ratio, which showed the influence of the axial velocity. At the higher advance ratio the measured swirl at the sides of the motor tube decreased which means that the calculated results were more in line with those measured. The influence of the turbulence model was also investigated at an instantaneous blade position to avoid the influence of the averaging over one revolution. The investigation did not show a significant difference, that would motivate a more time consuming turbulence model and hence the k-ω model was used in all the other investigations.

For plane one, which was located in front of the first structure, both URANS and BEM predicted the overall distribution quite well, what neither caught was the turbulent swirl at the sides of the motor tube.

For the second plane the URANS calculation predicted a clearly larger axial velocity than the BEM, which gave an over prediction for the URANS compared to the measurements.

The inflow angle was observed at 12 o'clock position for the first and 6 o'clock for the second plane. These locations represented the leading edge of the strut and the fin. Both URANS and BEM predicted the inflow angle distribution close to the average measured one at the 12 o'clock position on plane one. On the second plane the calculated magnitude and form were closer to each other between the URANS and the BEM, than to the measured distribution. Here the form of the measured distribution was of a clearly different form than the calculated.

On the third and fourth plane the influence of the pod housing is seen in the measurements. For the BEM calculations the housing has only minor influence on the axial components, but its presence can be noted in the velocity vectors. The URANS distribution is more in line with the measurements, however, the distribution and magnitude is larger on planes three and four. Here, the inflow angle predicted from the URANS shifts on the upper and lower half of the propeller disc, which could be intuitively expected. However, for the measured results this does not happen, on the contrary, the inflow comes from the same direction for both the upper and the lower part. The inflow shifts from the right on plane three to an inflow from the left on plane four. This seems to be due to the difference in the propeller used for the measurement.

The BEM method works well to predict the performance of the propeller, it lacks some accuracy for the flow behind it. The method gives a good indication of how the flow behaves in front of the stationary objects, but behind there are more fluctuations. On the other hand the URANS calculations give a slightly better picture of the overall flow in front of stationary object. And the solution behind the object is stable. However, neither of the calculation methods predicted the swirls that were measured at the sides of the motor tube.

Taken that this was a first investigation on the accuracy of simulating the slip stream from a propeller over the Azipod housing using both measurements and calculations the results were adequate. There are error margins in all methods, but they are difficult, if not, impossible to define. Taken the principle of the BEM it was expected to be able to predict the inflow angle for the leading edges of the strut and fin. The method produced a reasonable inflow angle for the12 and 6 o'clock positions in addition to producing a reasonable

distribution at the two first investigation planes. With the URANS calculations the expectation was to be able to get a general feel for the whole calculation volume. The calculation results matched what was expected, but what could not be predicted was the behavior around the fin and the swirls at the sides of the motor tube. Since the mesh was generated for standard open water calculations, it might leave room for improvement. However, the mesh consisted of 6 million cells and a reasonable y+ value on the Azipod surfaces, so some indication of the missed velocity behavior would have been expected. On the other hand the measurements also contain errors. The measurement planes were difficult to light and photograph, so to get the whole plane a right- and a left handed propeller were used, which introduced a difference in the geometrical accuracy. Additionally, the reflections from the Azipod housing could affect the measurements by introducing non existing velocity components. But the swirls at the sides of the motor tube seem to be too constant and regular between the measurements to be explained by a measurement error.

REFERENCES

Bosschers J (2009) "Procal v2.0 theory manual". Internal CRS document.

Felli M, Falchi M, Pereira F (2011) "Inverstigation of the Flow Field around a Propeller-Rudder Configuration: On-Surface Pressure Measurements and Velocity-Pressure-Phase-Locked Correlations". Second International Symposium on Marine Propulsors – SMP'11, Hamburg, Germany, June, 2011

Mikkola T, Hanhirova K, Hämäläinen R (2012) "Experimental Study of Propeller-Rudder Interaction Using Particle Image Velocimetry". Conference on Modelling Fluid Flow (CMFF'12)- The 15th International Conference on Fluid Flow Tehnologies, Budabest, Hungary, September 4-7, 2012

Roosenboom E, Sturmer A, Schröder A (2009) "Comparison of PIV measurements with unsteady RANS calculations in a propeller slipstream". 27th AIAA Applied Aerodynamics Conference, San Antonio, Texas, USA, June 22-25, 2009

StarCCM+ UserGuide 9.02. CD-adapco 2014.